Soft Matter

A spectroscopic and molecular dynamics study on the aggregation process of a long-acting lipidated therapeutic peptide: the case of Semaglutide

Journal:	*Soft Matter*
Manuscript ID	SM-ART-05-2020-001011
Article Type:	Paper
Date Submitted by the Author:	31-May-2020
Complete List of Authors:	Venanzi, M.; University of Rome Tor Vergata, Department of Chemical Science and Technologies SAVIOLI, MARCO; University of Rome Tor Vergata, Dept. of Chemical Science and Technologies Cimino, Rita; University of Rome Tor Vergata, Dept. of Chemical Science and Technologies Gatto, Emanuela; University of Rome Tor Vergata, Department of Chemical Science and Technologies Palleschi, Antonio; University of Rome Tor Vergata, Dept. of Chemical Science and Technologies Ripani, Giorgio; University of Rome Tor Vergata, Dept. of Chemical Sciences and Technologies Cicero, Daniel; University of Rome Tor Vergata, Dept. of Chemical Science and Technologies PLACIDI, ERNESTO; University of Rome La Sapienza, Dept. of Physics Orvieto, Federica; IRBM Bianchi, Elisabetta; IRBM

ARTICLE

A spectroscopic and molecular dynamics study on the aggregation process of a long-acting lipidated therapeutic peptide: the case of Semaglutide

Received 00th January 20xx,
Accepted 00th January 20xx

DOI: 10.1039/x0xx00000x

M. Venanzi,[a]* M. Savioli,[a] R. Cimino,[a] E. Gatto,[a] A. Palleschi,[a] G. Ripani,[a] D. Cicero,[a] E. Placidi,[b] F. Orvieto,[c] E. Bianchi[c]

The aggregation properties of Semaglutide, a lipidated peptide drug agonist of the Glucagon-like peptide 1 receptor recently approved for treatment of diabetes type 2, have been investigated by spectroscopic techniques (UV-Vis absorption, steady-state and time-resolved fluorescence, electronic circular dichroism) and Molecular Dynamics simulations. We show that in the micromolar concentration region, in aqueous solution, Semaglutide is present as monomeric and dimeric species, with a characteristic monomer-to-dimer transition occurring at around 20 μM. The lipid chain stabilizes a globular morphology of the monomer and dimer species, giving rise to a locally well-defined polar outer surface where the lipid and peptide portions are packed to each other. At very long times, these peptide clusters nucleate the growth of larger aggregates characterized by a blue luminescence and a β-sheet arrangement of the peptide chains. The understanding of the oligomerization and aggregation potential of peptide candidates is key for the development of long acting and stable drugs.

Introduction

Peptides represent a unique class of pharmaceutical compounds able to target protein-protein interactions where large and shallow surface areas are considered that cannot be easily targeted by conventional small molecules drugs.

Peptides are intrinsic signalling molecules for many physiological functions. In particular, in the case of the peptide G protein-coupled receptor (GPCR), the receptor/peptide hormone interaction site is quite large and requires specific conformational changes for signal transduction. Peptide therapeutics represent a unique opportunity for the cases where high selectivity and strong receptor affinity are required. [1,2] To this purpose novel strategies allow now to overcome the well-known liabilities of peptides, such as low metabolic stability, high clearance rates due to rapid renal filtration and low bioavailability.

In particular, different approaches allow for the modulation of the pharmacokinetic profile through the incorporation of non-natural amino acids and, most importantly, with the derivatization/ conjugation of half-life extension moieties, such as fatty acids [3] or cholesterol [4,5], that promote complexation with plasma proteins such as human serum albumin (HSA) or promote self-assembly to form larger structures. Peptides bound to HSA are sterically shielded from proteolytic degradation and the relatively large size of HSA (66 kDa) protects against rapid renal filtration.

The mechanism underlying the extended half-life of lipidated peptides involves both albumin binding and protraction of absorption by oligomerization. The first lipidated pharmaceuticals that were developed were analogues of the natural peptide hormones, insulin and Glucagon-like peptide 1 (GLP-1). The molecules differed in the type of fatty acids and for the kind and length of hydrophilic spacers such as γGlu or PEG2 (8-amino-3,6-dioxaoctanoic acid) between the peptide sequence and the fatty acid, so to modulate affinity to HSA, oligomerization and target receptor potency. Two successful examples for lipidated GLP-1 analogues are Liraglutide, [6] and Semaglutide. [7]

GLP-1 is a 30 amino acid hormone controlling the glucose levels by stimulating pancreatic secretion of insulin.[8] GLP-1 undergoes a self-limiting action, inhibiting the insulin production when the glucose reaches normal levels in the blood, therefore reducing hypoglycemia risks. Unfortunately, its residence time in the plasma is usually very short (1-2 minutes) due to fast enzymatic degradation by dipeptidyl-peptidase 4 (DPP-IV). [9]

Liraglutide is a once daily analogue that is approved for antidiabetic and obesity therapies. Starting from the natural GLP-1, extensive structure activity relationship studies led to: a) the identification of most tolerable positions for fatty acid derivatization; b) optimization of the spacer, such as γGlu, to compensate for the lack of the acidic group when the fatty acid is amidated to a Lys side chain; c) length of the fatty acid, with

[a] Dept. of Chemical Science and Technologies, University of Rome Tor Vergata, via della Ricerca Scientifica 1, 00133 Rome, Italy.
[b] Dept. of Physics, University of Rome 'La Sapienza', P.le Aldo Moro 5, 00185 Rome, Italy.
[c] Peptide and Small Molecule R&D Department, IRBM SpA, via Pontina KM 30,600, 00071 Pomezia, Italy.

Electronic Supplementary Information (ESI) available: Optical spectroscopy characterization of SMG aggregation process (Figures S1-S4; Tables T1-T2; Size distribution of SMG nanostructures imaged by AFM (Fig.S5-S7); Pasternack modelling of SMG long-time aggregation. See DOI: 10.1039/x0xx00000x

the finding that only lipid above a certain length (> C12) could translate to half-life longer than 10 hours (subcutaneous route). [10]

Liraglutide has a Lys to Arg substitution at position 34 while Lys(26) is derivatized on its side chain through a γGlu spacer and a palmitoyl group. The presence of the C16 fatty acid promote binding to HSA and protracted absorption, resulting in an extended half-life in humans (11-15 h) by subcutaneous administration. [10]

Further improvement on the use of fatty acids for the conjugation to peptides as half-life extending approach, was recently achieved with the implementation of fatty diacids for derivatizing peptides with a long carbon chain ending at one terminus with a free carboxylate (C16-OH, C18-OH, C20-OH). The presence of the carboxylate group on the fatty acid enables an improved interaction with HSA resulting in an extended half-life of one week in humans such as for Semaglutide, a new GLP-1 analogue. [7]

The long retention times of lipidated peptides in the blood have been explained by enhanced resistance to renal secretion promoted either by the formation of micelle-like peptide nanostructures, or with the association to HSA. As the lipidated peptide is thought to bind HSA exclusively as a monomeric species, the two mechanisms appear to be competitive, as the binding to HSA subtracts peptide monomers to the aggregation equilibria leading to micellization. [11,12] Also self-association to form either amorphous aggregates or highly structured fibrillar species may limit their use, therefore careful inspection on this propensity should be part of the discovery process. [13]

The chemical structure of Semaglutide in the following denoted as SMG for brevity, is reported in Scheme 1. In SMG, an Ala residue in position 8 was substituted with a non-metabolic residue, i.e. α-amino isobutiric acid (Aib), and the side chain of Lys(26) was derivatized by a spacer comprising two PEG2 groups, a γ-Glutamyl residue, and a C18-OH lipid chain. The fat lipid chain is thought to increase the affinity of Semaglutide to HSA, while the non-metabolic Aib residue is expected to increase its resistance to enzymatic degradation by DPP-IV. [7]

Aim of this contribution is to study the aggregation properties of SMG in aqueous solutions, determining its critical aggregation concentration and characterizing by spectroscopic methods and Molecular Dynamics simulations the formation of the small supramolecular structures nucleating the growth of large SMG aggregates. The presence in the SMG peptide chain of two fluorescent amino acids, i.e. Trp (W) and Tyr (Y), allowed us to apply optical spectroscopy techniques to characterize the aggregation properties of SMG.

Materials and Methods

Synthesis of Semaglutide, The sequence His-Aib-Glu-Gly-Thr-Phe-Thr-Ser-Asp-Val-Ser-Ser-Tyr-Leu-Glu-Gly-Gln-Ala-Ala-Lys(C18acid-γ-Glu-PEG2-PEG2)-Glu-Phe-Ile-Ala-Trp-Leu-Val-Arg-Gly-Arg-Gly-OH, was synthesized by stepwise solid phase assembly on a 2-chlorotrityl chloride resin using Fmoc/tBu strategy. The first amino acid Fmoc-Gly-OH (1 equivalent) was loaded on the resin by incubation in a DMF solution in the presence of 2 equivalents of N, N-diisopropylethylamine. The sequence assembly was performed on a Symphony (Protein Technologies Inc.) synthesizer with Lys(26) incorporated as Fmoc-Lys(Dde)-OH so to afford side chain derivatization on solid phase with two PEG2 (8-amino-3,6-dioxaoctanoic acid) units, γ-glutamic acid and saturated fatty diacid C18-OH. The cleavage from resin and side chain deprotection was performed by incubation with a TFA solution containing 5% phenol, 2.5% triisopropylsilane and 5% water. The crude peptide was precipitated in methyl-tert-butyl ether. The lyophilized peptide crude was purified by reverse phase chromatography on a C4 column (Reprosil, 200Å, 5µm, Dr. Maisch GmbH) on a Waters HPLC system. The analysis was performed by ultra-high performance liquid chromatography – UV- mass spectrometry (UPLC-UV-MS) on a Waters Acquity UPLC system equipped with a Waters BEH130 C4 (2.1x100 mm, 1.7µm, at 45°C) column. Analysis was typically performed over 2, 5 or 10 min runs as required applying linear gradients of acetonitrile in H_2O, 0.1% TFA with a flow rate of 0.4 mL/min and UV detection at 214 nm. Mass analysis was performed on a Waters SQ or SQ2 detector with electrospray ionization in positive ion detection mode. The scan range of the mass-to-charge ratio was 1000-3000.

UV-Vis absorption measurements were carried out by a Cary100 Scan spectrophotometer using asymmetric quartz cuvettes with 4/10 mm optical paths at room temperature (25°C). All the absorption spectra were corrected by subtracting the absorption spectrum of the buffer solution in the same wavelength range (200-350 nm). Concentration of freshly-prepared solutions was obtained from the Lambert-Beer equation, assuming the molar extinction coefficient at λ=280 nm $\varepsilon(280)$=7200 M^{-1} cm^{-1}, as a result of the sum of the Tryptophan [$\varepsilon(280)$=5600 M^{-1} cm^{-1}] and Tyrosine [$\varepsilon(280)$=1600 M^{-1} cm^{-1}] molar extinction coefficients.[14]

Steady-state fluorescence experiments were carried out on a thermostatted (25°C) 4/10 mm asymmetric quartz cuvette by a Fluoromax-4 spectrofluorometer (Horiba, Jobin Yvon) with single photon counting (SPC) detection. Fluorescence emission spectra were measured at the excitation wavelength of 280 and 295 nm, while the associated excitation spectra were measured at the emission wavelength of 350, 360 and 410 nm. 2D emission/excitation fluorescence maps were obtained by collecting 20 emission spectra carried out by varying the excitation wavelengths between 250 and 300 nm, and the emission wavelengths between 300 and 500 nm.

Fluorescence anisotropy measurements were carried out on the same apparatus equipped with automatically-driven Glan-Thomson polarizers. The position of the excitation and emission polarizers was calibrated using a Ludox scattering solution. The anisotropy coefficient r was obtained by the equation:

$$r = \frac{I_{\parallel} - I_{\perp}}{I_{\parallel} + 2I_{\perp}} \quad (1)$$

Where $I_{//}$ and $I_{\perp}$ are the fluorescence intensities measured where the excitation and emission polarizers are each other oriented in a parallel or perpendicular position, respectively.

Rotational correlation times were obtained through the Perrin

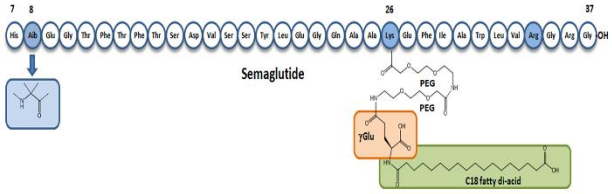

Scheme 1. Schematic view of Semaglutide (**SMG**) structure

equation for a spherical rotor [15]

$$\frac{r_0}{r} = 1 + \frac{\tau}{\theta} \quad (2)$$

where r_0 is the limit anisotropy coefficient at t=0, an intrinsic property of the fluorophore, τ the fluorescence lifetime of the fluorophore, and θ the rotational correlation time. The latter is connected to the hydrodynamic volume V_h of a spherical rotor through the Einstein-Smolukovski equation [15]:

$$\theta = \frac{\eta V_h}{RT} \quad (3)$$

where η is the solution bulk viscosity.

The critical aggregation concentration (*cac*) of SMG was determined through the pyrene fluorescence assay, measuring the relative intensities of the first [$S_2(v=0) \rightarrow S_0(v=0)$, λ_{max}=373 nm)] and third [$S_2(v=0) \rightarrow S_0(v=1)$, λ_{max}=384 nm] vibronic transitions. [16] The titration experiment was carried out adding at each step 25 µl of 66 µM SMG to a 1 µM pyrene solution (phosphate buffer, pH 8, 25°C).

Time-resolved fluorescence experiments were carried out on a thermostatted (25°C) asymmetric (4/10 mm) quartz cuvette with an EAI Spec-ps (Edinburgh Analytical Instruments) spectrofluorimeter with time-correlated SPC detection. Excitation at 295 and 344 nm was obtained by two Hamamatsu diode lasers (pulse width 1 ns). Experimental fluorescence time decays were analyzed by an iterative reconvolution method, using a multiexponential fitting function, i.e.

$$I(t) = \sum_i \alpha_i exp\left(-\frac{t}{\tau_i}\right) \quad (4)$$

where α_i are the pre-exponential weighting factors, proportional to the abundance of the *i*th species at t=0, and τ_i, the lifetime of the *i*th time decay component.

Circular dichroism experiments were carried out by a Jasco J–1500 CD spectropolarimeter (Jasco International Co.) in the wavelength range from 190 to 250 nm, at 25°C using an equipped Peltier thermostatted cell holder (PTC-510). Measurements were performed in a 0.1 cm quartz cuvette (Hellma, Mühlheim, Germany) using a scan speed of 50 nm min^{-1}, a bandwidth of 1 nm, integration time of 1 s. Each spectrum was obtained as the average of 4 repeated scans.

Atomic Force Microscopy experiments were carried out in air at room temperature on a Veeco Multiprobe IIIa instrument (Santa Barbara, CA). The AFM measurements were carried out in tapping mode on films obtained by drop casting micromolar aqueous (phosphate buffer, pH 8) solutions of SMG on mica, and incubating for 18 hours in a dryer. For the AFM measurements, a Si super sharp tip, functionalized by carbon flake was used (curvature 1 nm, elastic constant 5 N/m, resonance frequency 150 kHz).

MD simulations of aggregates have been performed placing 4 SMG molecules in a 5.13x13.38x8.43 nm^3 box, with 18145 water molecules and 16 Na^+ counter-ions to neutralize the total charge. All the simulations have been performed using the gromos53a6-FF force field [17] (modified for LysP chain) with the MD simulation package GROMACS16 MPI.[18] Time steps of 2 fs have been used for the equilibration and production runs. The equilibrium temperature (300 K) was controlled by velocity rescaling with a coupling constant of 0.6 ps. Pressure was controlled by an isotropic Berendsen barostat [19] with a coupling constant of 1 ps and a reference external pressure of 1 atm. Lennard-Jones long range interactions were treated with a cut-off radius of 1.4 nm and coulombic interactions were calculated by the Particle Mesh Ewald method.[20] Three replicas of each system have been performed for 30 ns long simulations with different starting configurations.

Results

Aggregation of SMG at early times

The absorption spectrum of SMG in the near UV region (Figure 1) is characterized by the overlap of the π→π* (λ_{max}=205 nm) and n→π* (λ_{max}=280 nm) transitions of chromophores in the sequence (Scheme 1): the indole group of Trp(31) and the phenol group of Tyr(19).

From Figure 1 it can be observed that, in the SMG concentration region comprised between 20 and 30 µM, a hypochromic effect and a slight broadening of the π→π* transition takes place, as usually observed in aggregation phenomena promoted by the stacking of aromatic moieties. [1, 21, 22]

Fluorescence emission spectra of **SMG** were measured either at the excitation wavelengths of 280 nm, where both Trp and Tyr chromophores can be excited, and 295 nm, where Trp is

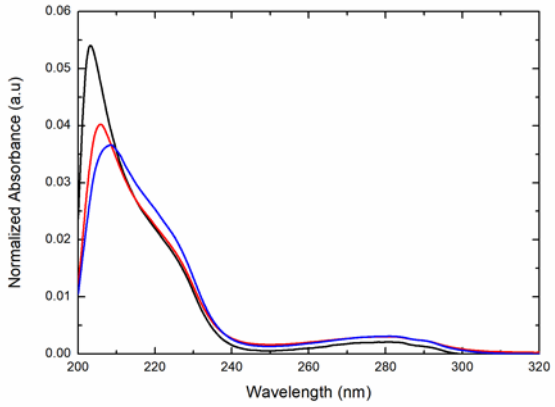

Figure 1. Absorption spectra of SMG in aqueous solution (phosphate buffer, pH=8). Black: 4 µM; red: 20 µM; blue: 30 µM. The spectra were normalized to unit area to emphasize differences in the shape.

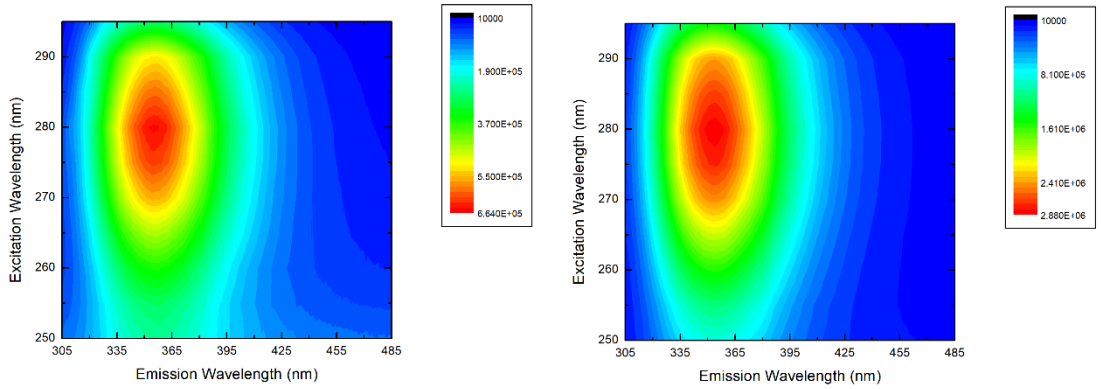

Figure 2. 2D emission/excitation fluorescence maps of SMG aqueous solutions (phosphate buffer, pH 8, T=25°C). Left: 4 µM; right: 30 µM.

selectively excited. Interestingly, the emission spectra obtained at the two excitation wavelengths closely overlap (ESI, Fig. S1), showing in both cases wavelength emission maxima peaked at λ=350 nm. In agreement with this finding, 2D emission/excitation fluorescence maps of freshly-prepared **SMG** solutions in the micromolar concentration region show the presence of a single emitting species, confirming the occurrence of a total Tyr*→Trp* energy transfer (Figure 2).

Fluorescence emission spectra, normalized by the absorbance at the excitation wavelength (λ_{ex}=295 nm), showed decreasing intensities with increasing the SMG molar concentration along the series 4 > 30 > 20 µM (ESI, Figure S2), strengthening the idea that an aggregation process takes place in the micromolar concentration region investigated, leading to quenching of the tryptophan emission.

Time resolved fluorescence measurements (λ_{ex}=295 nm, λ_{em}= 350 nm), carried out for different SMG concentrations, show that, at least, three exponential time components are necessary to adequately reproduce the experimental decays of the Trp fluorophore. Lifetimes and pre-exponential weights obtained from iterative deconvolution of the SMG fluorescence time decays in the concentration region comprised between 4 and 30 µM are reported in Table 1.

The data reported in Table 1 indicate that, at least in the micromolar region investigated, fluorescence time decays do not significantly depend on the SMG concentration. This finding suggests that the Trp fluorescence quenching is predominantly caused by ground-state interaction between the aromatic groups.

Steady-state fluorescence anisotropy measurements were carried out to determine the fluorescence anisotropy coefficient r, and, through the Perrin (Eq. 3) and Einstein-Smoluchowski (Eq. 4) equations, the rotational diffusion coefficient and hydrodynamic volume of SMG at different concentrations.

In Figure 3 we report the anisotropy coefficient r as a function of the temperature/viscosity ratio (T/η) measured for SMG water/glycerol 1:2 (v/v) solutions. Time decay parameters of SMG under the same experimental conditions are reported as ESI in Table T1.

It should be noted that the r *vs* T/η behaviour is highly non-linear, suggesting some conformational flexibility of the region. sampled by Trp. In the presence of segmental flexibility, the integrated anisotropy coefficient r can be described by the equation: [15]

$$r(\tau) = \frac{\alpha r_0}{1+\left(\frac{1}{\vartheta_F}+\frac{1}{\vartheta_S}\right)\tau} + \frac{(1-\alpha)r_0}{1+\frac{\tau}{\vartheta_S}} \qquad (5)$$

where ϑ_F and ϑ_S represent the fast and slow time components

Table 1. Lifetimes and pre-exponential weights obtained by iterative deconvolution of the **SMG** fluorescence time decay at different concentrations (phosphate buffer, pH 8, T=25°C; λ_{ex}=295 nm, λ_{em}= 350 nm).

[SMG] (µM)	α_1	τ_1 (ns)	α_2	τ_2 (ns)	α_3	τ_3 (ns)	<τ> (ns)
4	0.36	1.0	0.50	3.4	0.14	6.5	3.0
20	0.38	1.4	0.45	3.5	0.16	6.7	3.2
30	0.38	1.2	0.45	3.5	0.17	6.9	3.2

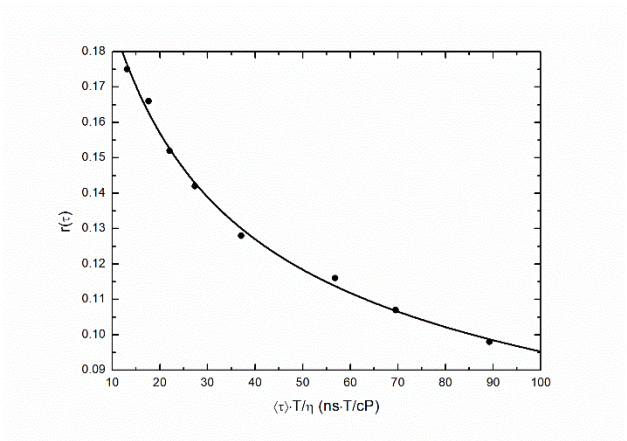

Figure 3. Anisotropy coefficient r of 20 µM **SMG** in water/glycerol 1:2(v/v) as a function of the temperature/viscosity ratio.

of the anisotropy time decay, associated to the local motion of the tryptophan residue and to the global rotation of SMG, respectively; α and (1-α) are the relative weights of the two rotational components. It should be noted that the anisotropy coefficient r is a functional of τ, the fluorescence lifetime of the fluorophore.

Substituting for the two ϑ_F and ϑ_S time components by the Einstein-Smoluchowski equation, we obtain:

$$r(\tau) = \frac{\alpha r_0}{1+\left(\frac{1}{V_F}+\frac{1}{V_S}\right)\frac{RT\tau}{\eta}} + \frac{(1-\alpha)r_0}{1+\frac{1}{V_S}\frac{RT\tau}{\eta}} \qquad (6)$$

where V_F and V_S are the hydrodynamic volumes of the spherical rotors associated to the fast and slow components of the anisotropy decay. The data reported in Figure 3 were fitted by Eq. 6, providing an r_0 value equal to 0.260. Interestingly, under these experimental conditions, i.e. high viscosity water/glycerol 1:2 solutions, the segmental flexibility accounts for around 30% of the overall rotational motion depolarizing the fluorescence anisotropy.

Fluorescence anisotropy coefficients measured at different SMG molar concentrations, i.e. 4, 20 and 30 μM, in pH 8 aqueous solutions are reported in Table 2. Using the average time decays and the limit anisotropy coefficient (r_0) determined above, and assuming that, under these low viscosity experimental conditions, the measured residual anisotropy is entirely ascribable to the SMG global rotation, the rotational correlation time (θ) and the hydrodynamic volume (V_h) can be obtained by Eqs. 2 and 3, respectively. Hydrodynamic radii at the different SMG concentrations, also reported in Table 2, were obtained by considering SMG as a rigid spherical rotor, i.e.

$$r_h = \sqrt[3]{\frac{3V_h}{4\pi}}. \qquad (7)$$

The increase of the hydrodynamic volume observed for increasing SMG concentrations suggests the formation of small oligomers at the higher concentrations investigated.

The critical aggregation concentration (*cac*) of SMG in a phosphate buffer solution (pH 8) was obtained by the well-established pyrene assay. The latter is based on the dependence of the ratio between the intensities of the first and third vibronic components (I_1/I_3) of the pyrene emission band on the environment polarity.[16] Specifically, when the pyrene is embedded in an apolar environment, the I_1/I_3 ratio strongly decreases. Increasing amounts of SMG were therefore added to a 1 μM pyrene aqueous solution, collecting the pyrene fluorescence emission spectra reported in ESI (Fig. S3). In Figure 4 the ratio of the intensities of I_1 and I_3 vibronic bands, centred at λ_{em}= 373 and 384 nm, respectively, is reported as a function of the SMG concentration (on a logarithmic scale).

Table 2. Anisotropy coefficients (r), rotational correlation time (Θ), hydrodynamic volume (V_h) and radii (r_h) at different SMG molar concentrations (phosphate buffer, pH 8, T=25°C; λ_{ex}=295 nm, λ_{em}= 350 nm).

[SMG] (μM)	r	Θ(ns)	V_h (nm^3)	r_h (Å)
4	0.072 ± 0.005	1.15 ± 0.06	5.3 ± 0.3	10.8 ± 0.1
20	0.089 ± 0.001	1.67 ± 0.06	7.7 ± 0.3	12.3 ± 0.1
30	0.096 ± 0.001	1.87 ± 0.06	8.6 ± 0.4	12.7 ± 0.1

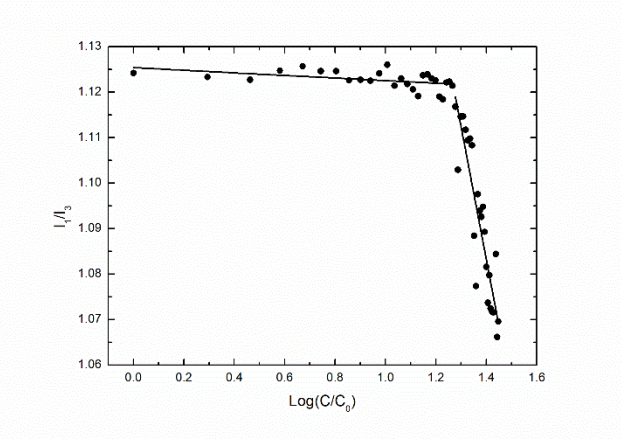

Figure 4. Ratio of the fluorescence intensities of the first (λ_{em}= 373 nm) and third λ_{em}= 384 nm) vibronic components as a function of the SMG concentration (log scale).

The *cac* can be determined at the intersection point of the two straight lines associated to the concentration regions where the pyrene fluorophore is fully exposed to water molecules or it is interacting with the peptide aggregate, respectively. From the data reported in Figure 4, it can be obtained a *cac* value of 20.2 μM, in agreement with the UV-Vis absorption and fluorescence results reported above that showed a similar abrupt change in the same concentration region.

Molecular Dynamics simulation. MD simulations have been carried out in order to investigate on the initial steps of SMG aggregation. During the 30 ns-long MD simulations three different structures have been observed, namely SMG monomers, dimers and trimers (Figure 5).

Larger structures were never observed during the sampled simulation time. During the simulation, the monomer showed a variety of secondary structures featuring coil (57%), beta-sheet (16%), bend (18%), and turn (6%) conformations. This conformational landscape is essentially conserved in the dimer and trimer structures.

In the structures reported in Figure 5, charged peptide side chains are fully exposed to the solvent, while the lipidated chains (LysP) appear folded and packed towards the peptide chains, and only partially accessible to water molecules. Noteworthy, the carboxylate groups of the lipid chains protrude towards the solvent-exposed surface, stabilizing the oligomer predominant structure. Interestingly, in all the simulations the side-chain phenyl group of Phe(6) remains rather close to the indole group of Trp(25). Besides that, the side-chain groups of the aromatic residues appear to be tightly arranged in the oligomerized structures, as also suggested by the observed hypsochromic effect shown by the UV absorption spectra and the Trp fluorescence emission quenching.

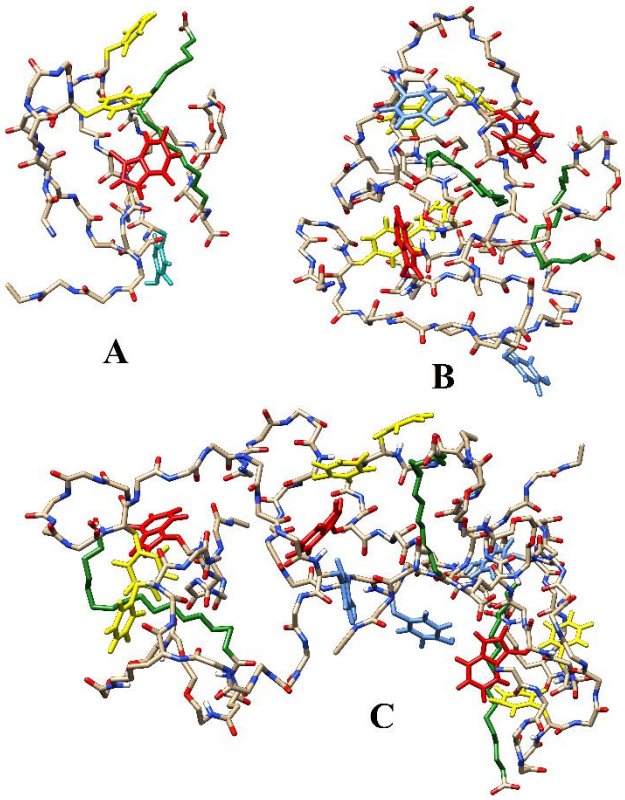

Figure 5. Molecular structures of SMG monomer (A), dimer (B) and trimer (C) as provided by MD simulation. The aromatic groups were reported in red (Trp), yellow (Phe) and light blue (Tyr). LysP sidechains are shown in green.

These findings allowed us to conclude that the fast folding of a single molecule is rapidly followed by the formation of SMG dimers and, sporadically, trimer oligomers. Gyration (r_g) and hydrodynamic (r_h) radii of SMG monomer, dimer and trimer were obtained from GROMACS tools (Table 3). Specifically, r_h was obtained by Eq. 8 [20]

$$r_h = \langle r_{ij}^{-1} \rangle^{-1} \qquad (8)$$

where i and j are indices running on the C$^{\alpha}$ atoms and carbon atoms of LysP separated by two bonds.

Autocorrelation rotational times were obtained by the inverse of the angular velocity of the orientation vector, considering each aggregate as a rotating ellipsoid (Figure 6).

The comparison between the calculated hydrodynamic radii with the experimental values reported in Table 2, indicates that, below the *cac*, SMG monomers, characterized by a r_h of 10.8 (fluorescence anisotropy) - 10.4 Å (MD) predominate, while, above the *cac,* dimeric clusters [r_h=12.7 (fluorescence anisotropy) - 12.8 Å (MD)] prevail. These findings led us to conclude that: (i) at the critical aggregation concentration determined by the pyrene assay, i.e. 20 µM, a monomer-to-dimer transition takes place, and (ii) the structures predicted by MD simulations faithfully reproduce the dimensions of the small clusters nucleating the growth of SMG aggregates.

The structures reported in Figure 6 clearly highlight the role of the LysP lipid chain that, interacting with the peptide backbone, gives rise to a locally well-defined apolar outer region that protrudes from the peptide assembly.

Table 3. Rotational autocorrelation times (Θ), gyration (r_g) and hydrodynamic (r_h) radii of **SMG** monomers, dimers and trimer.

system	Θ(ns)	r_g (Å)	r_h (Å)
Monomer	1.12 ± 0.25	9.9 ± 0.5	10.4 ± 0.3
Dimer	2.04 ± 0.86	12.1 ± 0.3	12.8 ± 0.3
Trimer	5.38 ± 2.35	21.0 ± 2.0	17.0 ± 0.1

Long-time aggregation of SMG

Following the SMG aggregation process, we noticed that both the absorption and fluorescence spectra varied significantly day by day. In particular, the absorption spectra of a SMG 20 µM solution showed a strong decrease and a wide broadening of the π→π* and n→π* absorption bands associated to the indole (Trp) and phenol (Tyr) aromatic groups (ESI, Figure S4).

The associated fluorescence emission spectra initially showed the same effect, i.e. decreased intensities and broadening of the

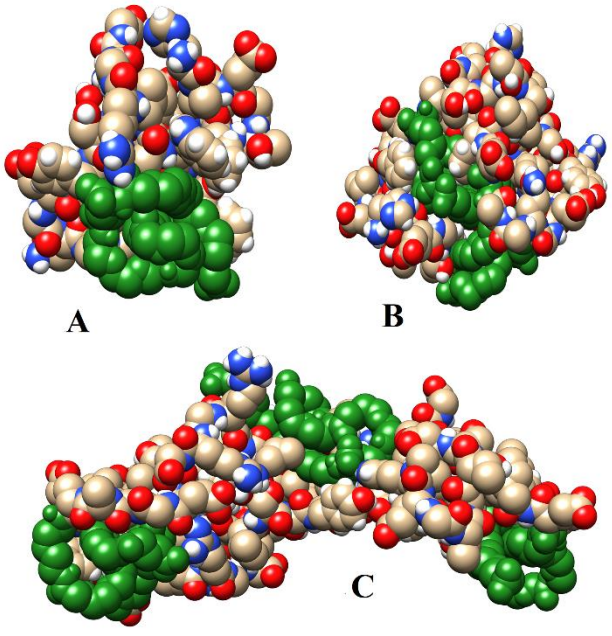

Figure 6. Filled-sphere representation of SMG monomer (A), dimer (B) and trimer (C) from MD simulation. LysP sidechains are shown in green.

ARTICLE

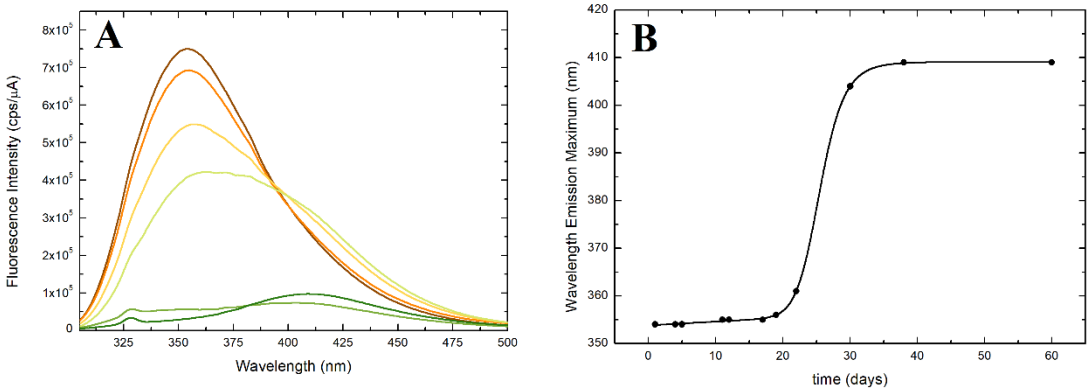

Figure 7 A: Emission spectra of SMG 20 μM (phosphate buffer, pH 8) at different times (λ_{ex}= 295 nm). B: wavelength emission maxima of SMG 20 μM at different times (days). The solid line was obtained fitting the experimental data by the model of Pasternack et al. [23].

emission band peaked at around 360 nm. Besides that, at very long times (days), a new emission feature appears at longer wavelength, characterized by a fluorescence maximum at around 410 nm (Figure 7A).

In Figure 7B, the wavelength emission maxima at different times (days) of 20 μM SMG aqueous solutions are reported. The solid line in Figure 7B was obtained fitting the experimental data by the model of Pasternack et al. [23].

The latter describes aggregation as a fractal autocatalytic process, characterized by a time dependent rate constant. In this kinetic approach, the rate-determining step is the achievement of a critical concentration of small clusters, formed by *m* monomers, and nucleating the autocatalytic growth of large aggregates. In the Pasternack model, the catalytic rate constant, k_c, scales with the mean cluster size, s(t), which in turn scales as a power law dependence on time, i.e. $s(t) \sim t^n$. The time dependent rate constant is therefore written as:

$$k(t) = k_0 + k_c(k_c t)^n \qquad (9)$$

to account for the non-catalytic (k0) and catalytic (kc) pathways. The integrated equation rate is readily written as:[23]

$$\frac{([M]-[M_i])}{([M_0]-[M_i])} = (1 + (m-1)\{k_0 t + (n+1)^{-1}(k_c t)^{n+1}\})^{-\frac{1}{m-1}} \qquad (10)$$

Where [M], $[M_0]$ and $[M_i]$ are the monomer concentration at time, t, t=0, and t=∞, respectively.

We adapted Eq. 10 to fit the data reported in Figure 7B, obtaining: k_0 = (1.5±0.4)·10^{-3} d^{-1}, k_c=(4.72±0.04)·10^{-2} d^{-1}, m=2.1±0.6, n=14±3. Details of the fitting procedure are reported as ESI.

Notably, the value obtained for the m parameter, i.e. the number of monomers forming the clusters, closely parallel the results of MD simulations.

The relative high value of n indicates that a strongly cooperative process is taking place, as usually found in hierarchical self-assembly. [24]

SMG aggregation should therefore occur through the following steps: (i) a fast oligomerization step leading to small peptide clusters (predominantly SMG dimers), followed by (ii) a very long delay time reaching a critical concentration, after which (iii) a fast and highly cooperative step involving the formation of mesoscopic (micrometric) structures, characterized by a faint blue luminescence.

In Figure 8 we reported the fluorescence emission spectra of aged solutions of SMG (phosphate buffer, pH 8) at λ_{ex}=295 nm (Figure 8A) and λ_{ex}=350 nm (Figure 8B), together with the fluorescence excitation spectra at λ_{em}=420 nm (Figure 8C).

It appears that excitation of the indole group at λ_{ex}=295 nm gives rise to a complex emission band, characterized by a shorter wavelength component, peaked at 330 nm, typical of the tryptophan monomer emission, and a longer wavelength component, peaked at around 410 nm. The latter mainly originates from a characteristic absorption peaked at around λ_{ex}=350 nm, as proved by the intense emission obtained by excitation at this wavelength (Figure 8B), and the excitation spectra reported in Figure 8C. Fluorescence spectra of different SMG solutions clearly show that the intensity of the longer wavelength component increases in competition with the

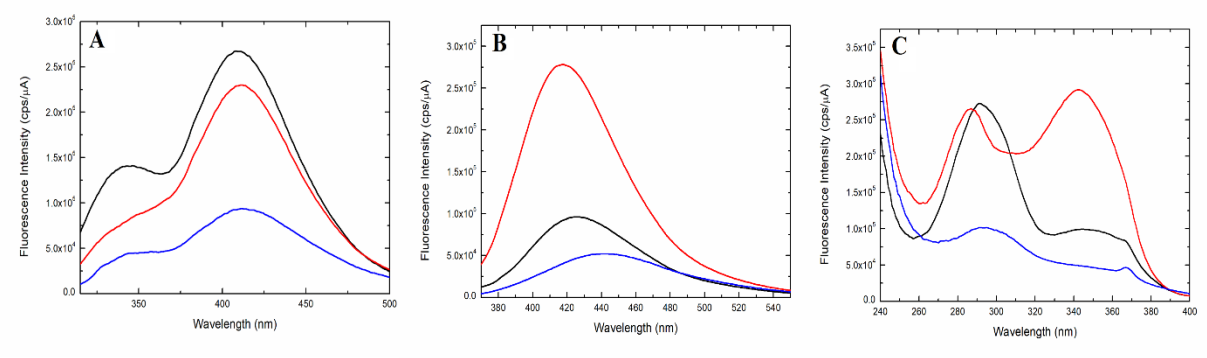

Figure 8. Fluorescence spectra of aged solutions of **SMG** (phosphate buffer, pH 8) at different times. A: Emission spectra at λ_{ex}=295 nm; B: Emission spectra at λ_{ex}=350 nm; C: Excitation spectra at λ_{em}=420 nm. The spectra were obtained by aged solutions of freshly-prepared 4 (black), 20 (red) and 30 μM (blue) SMG solutions.

tryptophan monomer emission.

Although this 'exotic' fluorescence has been found in several peptide systems, its origin at the moment is still fiercely debated. It has been proposed that this fluorescence originates from an extensive network of hydrogen bonds, like those realized in micrometric amyloid-like structures [25, 26], a quantum confinement effect in peptide nanostructures,[27] or semiconductor-like behaviour from micrometric structures.[28] Recently, Niyangoda et al. ascribed this blue luminescence to protein carbonyl groups.[29]

These findings led some researchers to propose this emission feature as a distinctive signal of the formation of amyloid structures, paving the way for the design of optical sensors capable of early diagnosis of neurodegenerative diseases.[30] However, the possibility of experimental artifacts due to diffused light contamination or oxidation of aromatic amino acids was recently advanced.[31] Formation of di-tyrosine cross-links was also shown to give rise to a weak fluorescence in the same region.[32]

Time-resolved emission measurements carried out at λ_{ex}=298 and 344 nm and λ_{em}=350 nm and 420 nm on SMG aged solutions, showed that the blue luminescence reported Figure 8 takes place in the nanosecond time region (ESI, Table T2), confirming the fluorescence nature of the emission. The recovered time decay parameters also suggest that the emitting excited state (or species) is beyond any doubt different from the species emitting in the UV region. Significantly, only a maximum of 10% of the signal can be ascribed to diffuse light contamination.

Interestingly, CD spectra of freshly-prepared and aged **SMG** aqueous solutions show that aggregation is coupled with a secondary structure transition from a mixture of random coil and helical conformations (Figure 9A), to a predominant β-sheet structure (Figure 9B).

In contrast with this evidence, fluorescence anisotropy measurements carried out on SMG aged solutions with λ_{ex}=298and 344 nm and λ_{em}=420 nm, showed that the blue emission reported in Figure 8 is characterized by a quite low anisotropy coefficient, independently on the peptide concentration (r=0.043 and 0.033 for 4 and 30 μM SMG solutions, respectively).

This finding clearly ruled out the diffuse light origin of the observed emission, in agreement with the results of time resolved experiments, but also suggests that the species emitting in the blue region of the spectrum are of small size.

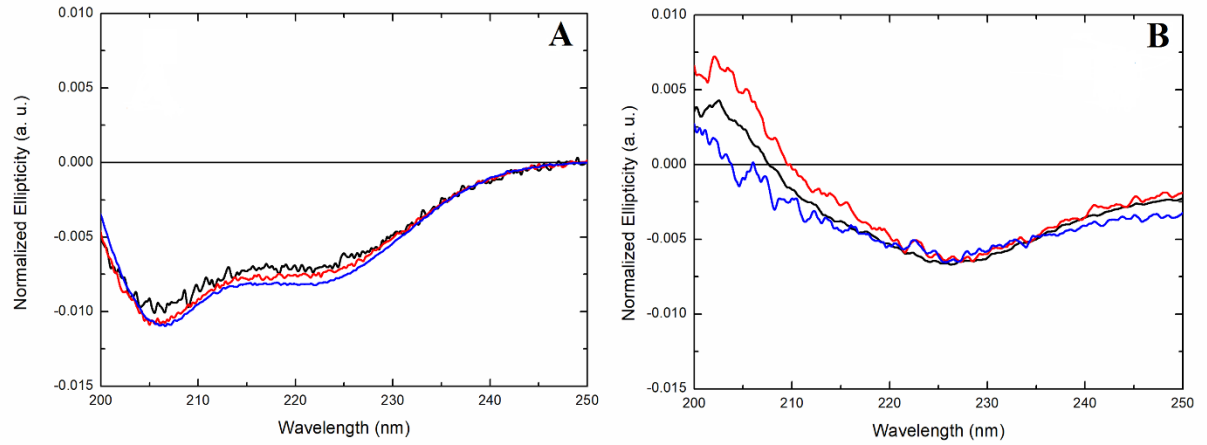

Figure 9. Circular dichroism spectra of freshly (A) and aged (B) SMG solutions. Black: 4 μM; red: 20 μM; blue: 30 μM.

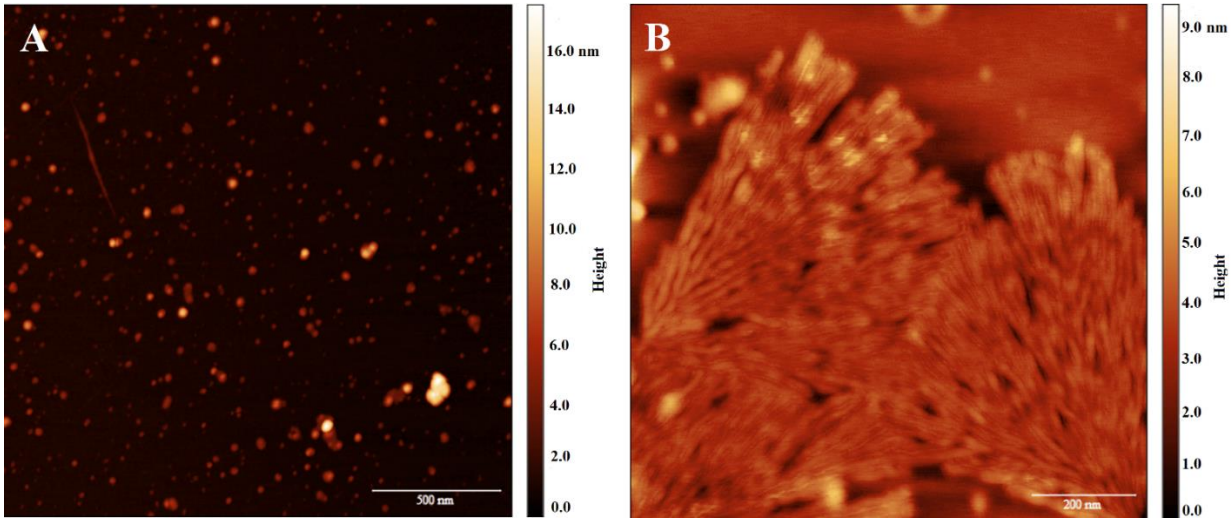

Figure 10. Atomic Force Microscopy images of SMG nanostructures deposited on mica from freshly-prepared (A) and aged (B) 30 µM SMG solutions (phosphate buffer, pH 8).

However, in the absence of information on the orientation of the absorption and emission dipoles of the species responsible for this 'exotic' fluorescence, no final conclusion can be drawn from these results.

A further evidence strengthens the idea that SMG forms large aggregates at very long times. AFM imaging of freshly-prepared 30 µM SMG solutions deposited on mica by drop casting, revealed the formation of small globular structures showing diameters of about 10-20 nm (Figure 10A). In the case of aged 30 µM SMG solutions, Gorgonian-like dendrimeric structures growing from rod building blocks, characterized by lengths of around 100 nm and widths of around 20 nm, can be easily spotted (Figure 10B). Size distributions of the SMG nanostructures imaged by AFM measurements, and deposited on mica from freshly-prepared and aged SMG solutions are reported as ESI (Figures S5-S7).

The observation of these fractal structures clearly recalls to the mind the interpretation of the aggregation process provided by the Pasternack model.

Conclusions

The aggregation properties of Semaglutide in the micromolar concentration region have been investigated by optical spectroscopy techniques and MD simulations. Under the applied experimental conditions, SMG features a very stable conformational landscape, characterized by a dynamic equilibrium between random coil and helical structures. MD simulations show that SMG attains a densely-packed globular morphology, with the peptide charged groups exposed to the solvent, and the fatty acid chain closely packed to the peptide backbone, thereby protecting the protein core. In this oligomeric structure SMG would be easily cleared by renal filtration with the equilibrium towards a monomeric species concurring to HSA complexation and prolonged half-life.

SMG was found to be quite soluble in aqueous solutions, forming at early times monomer species and small oligomers (dimers). Fluorescence anisotropy measurements and MD simulations consistently predict correlation times and hydrodynamic volumes of the monomer and dimer species.

At very long times (days) compelling spectroscopic evidences indicate that an aggregation process is steadily taking place, leading to the formation of an entirely new species, characterized by a faint blue luminescence signal, a β-sheet arrangement of the peptide chains, and, at the micrometric scale, Gorgonian-like morphologies.

The aggregation process was shown to be highly cooperative, as a result of the hierarchical character of peptide self-assembly nucleated by the small clusters (dimers and more rarely trimers) formed at early times.

The understanding of the oligomerization and aggregation potential of peptide candidates is key for the development of long acting and stable peptide drugs, where binding to human serum albumin has the key role as a half-life extending strategy, and the propensity to fibril formation should be counteracted as part of the drug development optimization process.[33]

Conflicts of interest

There are no conflicts to declare.

Acknowledgements

The technical assistance of Miss Erika Lunetta and Miss Alice Morganti (University of Rome Tor Vergata) in the optical spectroscopy experiments is gratefully acknowledged. This project received funding from the European Union Horizon 2020 research and innovation program under the Marie Skłodowska-Curie grant agreement no. 872233 (''PEPSA-MATE'').

References

.
1 J. L. Lau, M. K. Dunn, *Bioorg. Med. Chem.* 2018, **26**, 2700.
2 A.P. Davenport, C.C.G. Scully, C. de Graaf, A.J.H. Brown, J.J. Maguire, *Nat. Rev. Drug Discovery* 2020, in press.
3 P. Kurtzhals, S. Havelund, I. Jonassen, J. Markussen, *J. Pham. Sci.* 1997, **86**, 1365; E. M. Bech, S.L. Pedersen and K. J. Jensen, *ACS Med. Chem. Lett.* 2018, **9**, 577.
4 P. Ingallinella, E. Bianchi, N.A. Ladwa, Y.J. Wang, R. Hrin, M. Veneziano, F. Bonelli, T.J. Ketas, J.P. Moore, M.D. Miller, A. Pessi, *Proc. Natl. Acad. Sci. USA* 2009, **106**, 5801.
5 A. Santoprete, E. Capitò, P. E. Carrington, A. Pocai, M. Finotto, A. Langella, P. Ingallinella, K. Zytko, S. Bufali, S. Cianetti, M. Veneziano, F. Bonelli, L. Zhu, E. Monteagudo, D.J. Marsh, R. Sinharoy, E. Bianchi, A. Pessi, *J. Pept. Sci.* 2011, **17**, 270.
6 D. J. Drucker, A. Dritselis, P. Kirkpatrick, *Nat. Rev. Drug Discov.* 2010, **9,** 267.
7 J. Lau, P. Bloch, L. Schäffer, I. Pettersson, J. Spetzler, J. Kofoed, K. Madsen, L. B. Knudsen, J. McGuire, D. B. Steensgaard, H. M. Strauss, D. X. Gram, S. M. Knudsen, F. S. Nielsen, P. Thygesen, S. Reedtz-Runge, T. Kruse, *J. Med. Chem.* 2015, **58**, 7370.
8 B. Manandhar, J. M. Ahn, *J. Med. Chem.* 2015, **58**, 1020.
9 R. Meintein, B. Gallwitz, W. E. Schmidt, *Eur. J. Biochem.* 1993, **214**, 829.
10 L. B. Knudsen, P.F. Nielsen, P. O. Huusfeldt, N. L. Johansen, K. Madsen, F. Z. Pedersen, H. Thogersen, M. Wilken, H. Agerso, *J. Med. Chem*. 2000, **43**, 1664.
11 S. Janosch, C. Nicolini, B. Ludolph, C. Peters, M. Völkert, T. L. Hazlet, E. Gratton, H. Waldmann, R. Winter, *J. Am. Chem. Soc.* 2004, **126**, 7496.
12 Y. Wang, A. Lomakin, S. Kanai, R. Alex, S. Belli, M. Donzelli, G. B. Benedek, *J. Control Release* 2016, **241**, 25.
13 K. L. Zapadka, F. J. Becher, A. L. Gomes dos Santos, S. E. Jackson, *Interface Focus* 2017, **7**, 20170030.
14 R. Lettieri, M. D'Abramo, L. Stella, A. La Bella, F. Leonelli, L. Giansanti, M. Venanzi, E. Gatto, *Spectrochimica Acta* 2018, **195**, 84.
15 J. R. Lakowicz *Principles of Fluorescence Spectroscopy*, 2006, 3rd Ed., Springer, Singapore.
16 D. S. Karpovich, G. J. Blanchard, *J. Phys. Chem.* 1995, **99**, 3951.
17 C. Oostenbrink, A. Villa, A. E. Mark, W. F. van Gunsteren, *Comput. Chem.* 2004, **25**, 1656.
18 H. J. C.Berendsen, D. van der Spoel, R. van Drunen, *Comp. Phys. Comm.* 1995, **91,** 43.
19 H. J. C. Berendsen, J. P. M. Postma, W. F. van Gunsteren, A. Di Nola, J. R. Haak, *J. Chem. Phys.* 1984, **81**, 3684.
20 J. G. Kirkwood, *J. Polym. Sci.* 1954, **12**, 1.
21 M. Caruso, E. Placidi, E. Gatto, C. Mazzuca. L. Stella, G. Bocchinfuso, A. Palleschi, F. Formaggio, C. Toniolo, M. Venanzi, *J. Phys. Chem. B* 2013, **117**, 5448.
22 M. Caruso, E. Gatto, E. Placidi, G. Ballano, F. Formaggio, C. Toniolo, D. Zanuy, C. Aleman, M. Venanzi, *Soft Matter* 2014, **10**, 2508.
23 R. F. Pasternack, E. J. Gibbs, P. J. Collings, J. C. dePaula, L. C. Turzo, A. Terracina, *J. Am. Chem. Soc.* 1998, **120**, 5873.
24 B. B. Gerbelli, S. V. Vassiliades, J. E. U. Rojas, J. N. B. D. Pelin, R. S. N. Mancini, W. S. G. Pereira, A. M. Aguilar, M. Venanzi, F. Cavalieri, F. Giuntini. W. A. Alves, *Macrom. Chem. Phys*. 2019, **220**, 1900085.
25 A. Shukla, S. Mukherjee, S. Sharma, V. Agrawal, K. V. Radha Kishan, P. Guptasarma, *Archiv. Biochem. Biophys.* 2004, **428**, 144.
26 D. Pinotsi, L. Grisanti, P. Mahou, R. Gebauer, C. F. Kaminski, A. Hassanali, G. S. Kaminski Schierle, *J. Am. Chem. Soc.* 2016, **138**, 3046.
27 N. Amdursky, M. Molotskii, D. Aronov, L. Adler-Abramovich, E. Gazit, G. Rosenman, *Nano Lett.* 2009, **9**, 3111.
28 L. Laureana del Mercato, P. P. Pompa, G. Maruccio, A. Della Torre, S. Sabella, A. M. Tamburro, R. Cingolani, R. Rinaldi, *Proc. Ntl. Acad. Sci. USA* 2007, **104**, 18019.
29 C. Niyangoda, T. Miti, L. Breydo, V. Uversky, M. Muschol *PLos One* 2017, **12**, e0176983.
30 F. T. S. Chan, G. S. Kaminski Schierle, J. R. Kumita, C. W. Bertoncini, C. M. Dobson, C. F. Kaminski, *Analyst* 2013, **138**, 2156.
31 T. N. Tykhonova, N. R. Rovnyagina, A. Y. Zherebker, N. N. Sluchanko, A. A. Rubekina, A. S. Orekhov, E. N. Nikolaev, V. V. Fadeev, V. N. Uversky, E. A. Shirshin, *Archiv. Biochem. Biophys.* 2018, **651**, 13.
32 R. Aeschbach, R. Amadò, H. Neukom, *Biochim. Biophys Acta* 1976, **439**, 292.
33 I. W. Hamley, *Chem. Rev.* 2017, **117**, 14015.…

A spectroscopic and molecular dynamics study on the aggregation process of a long-acting lipidated therapeutic peptide: the case of Semaglutide.

M. Venanzi,* M. Savioli, R. Cimino, E. Gatto, A. Palleschi, G. Ripani, E. Placidi, D. Cicero, F. Orvieto, E. Bianchi

Electronic Supplementary Information

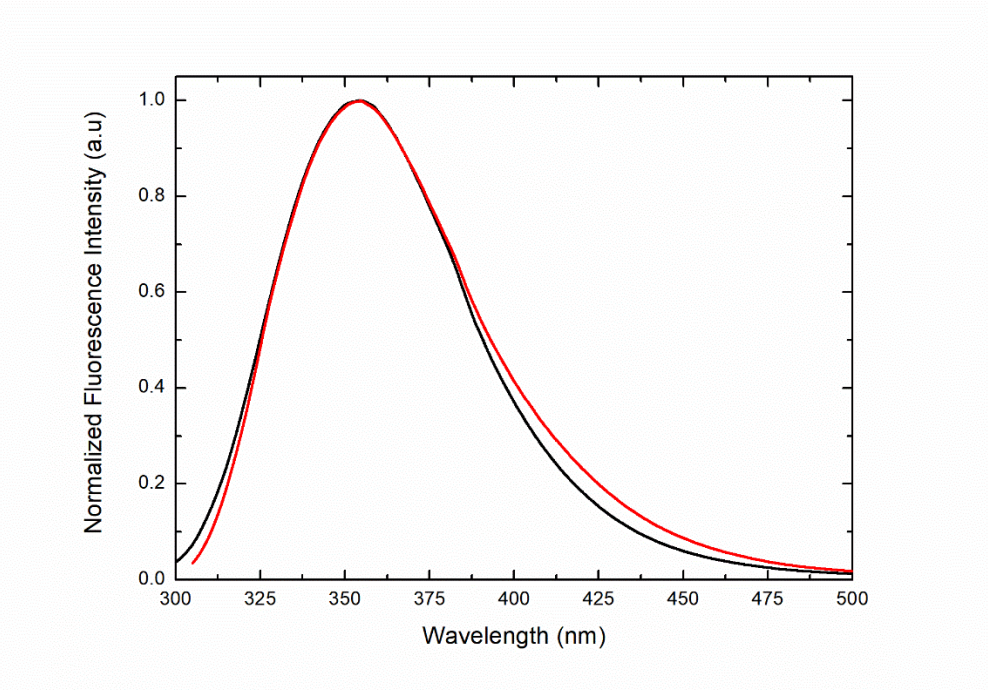

Fig. S1 Fluorescence spectra of SMG. Black line: λ_{ex}=280 nm; red: λ_{ex}=295 nm. The spectra were normalized to unit at the maximum to emphasize shape similarity.

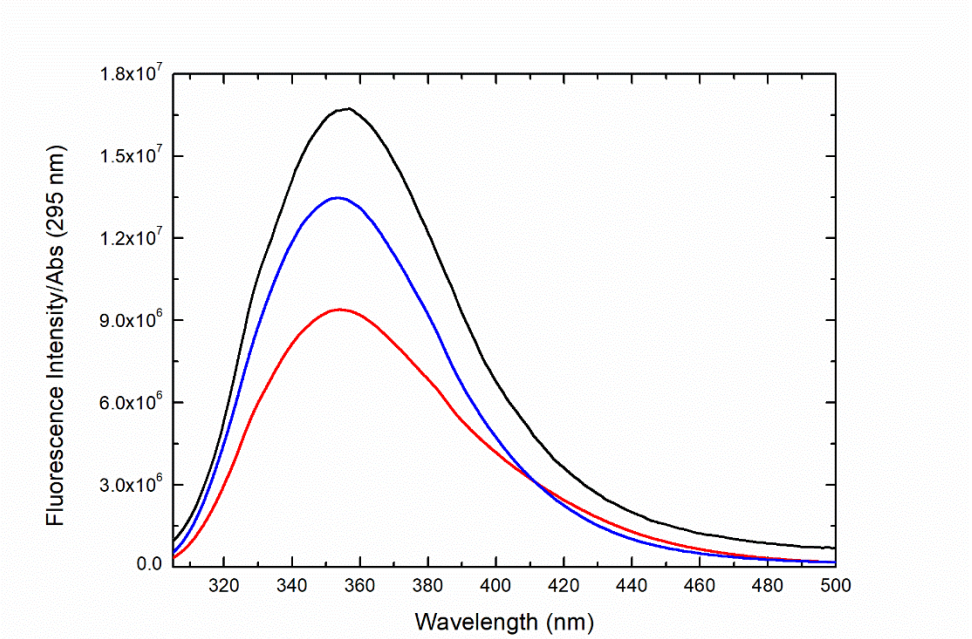

Fig. S2 Fluorescence emission spectra of SMG solutions (phosphate buffer, pH 8) normalized by the absorption at λ_{ex}=295 nm. Black line: 4 μM; blue: 30 μM; red: 20 μM.

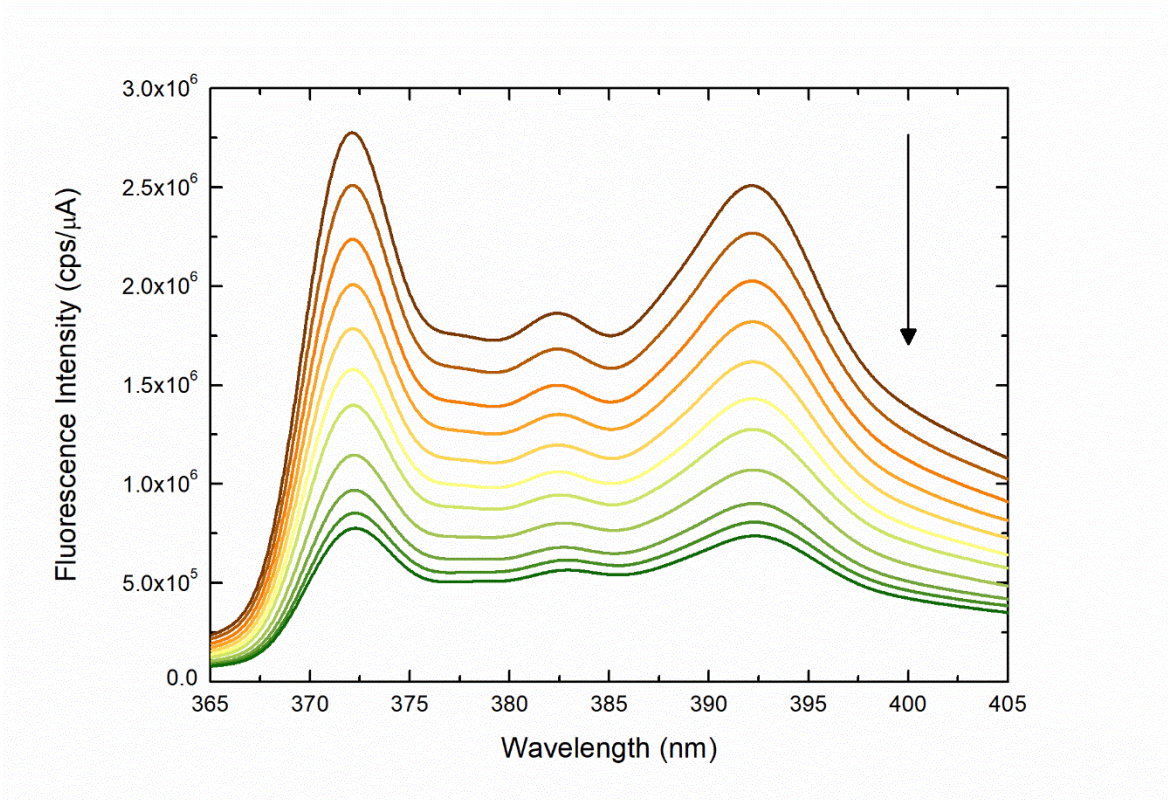

Fig S3. Fluorescence spectra of Pyrene (1μM) adding increasing aliquots (25 μl) of 66 μM SMG solution (phosphate buffer, pH 8, 25°C).

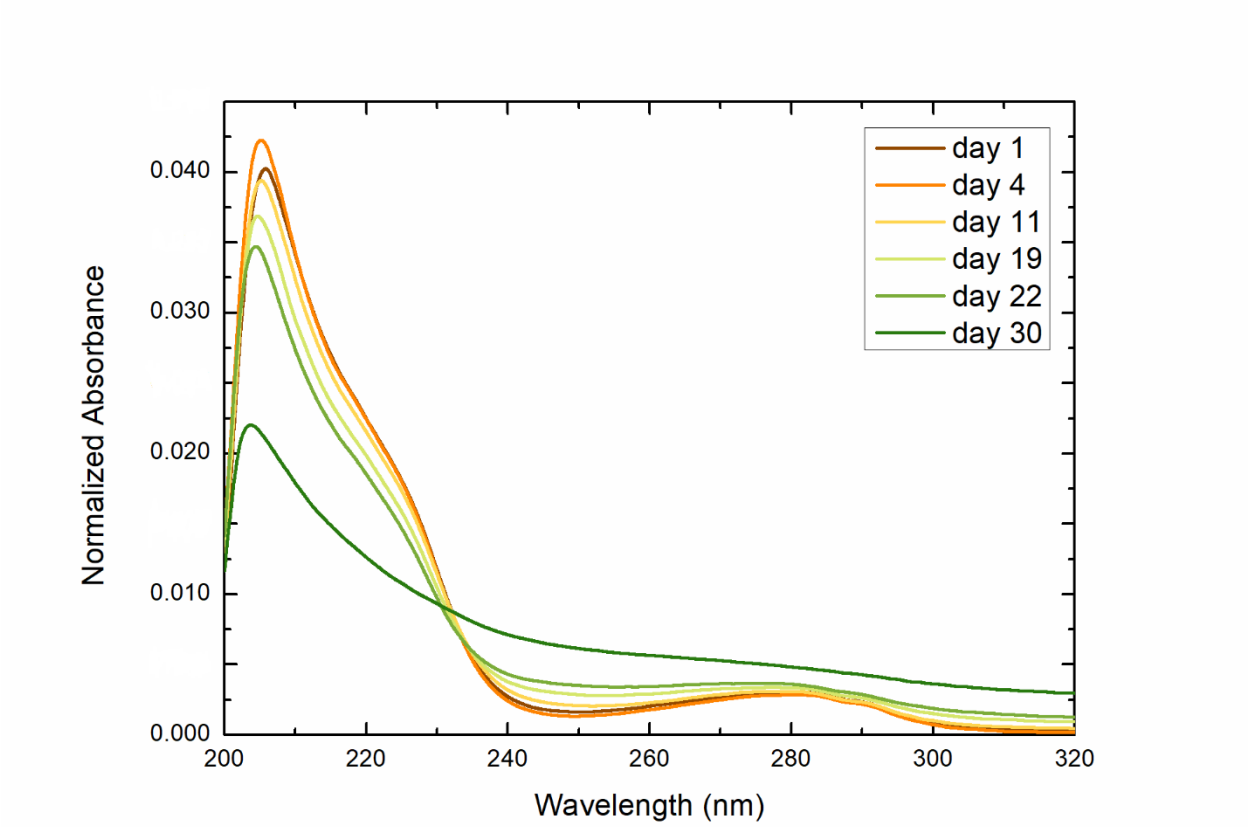

Fig. S4 Absorption spectra of SMG (phosphate buffer, pH 8, 25°C) at different times (days). The absorption bands were normalized to unit area for better comparison.

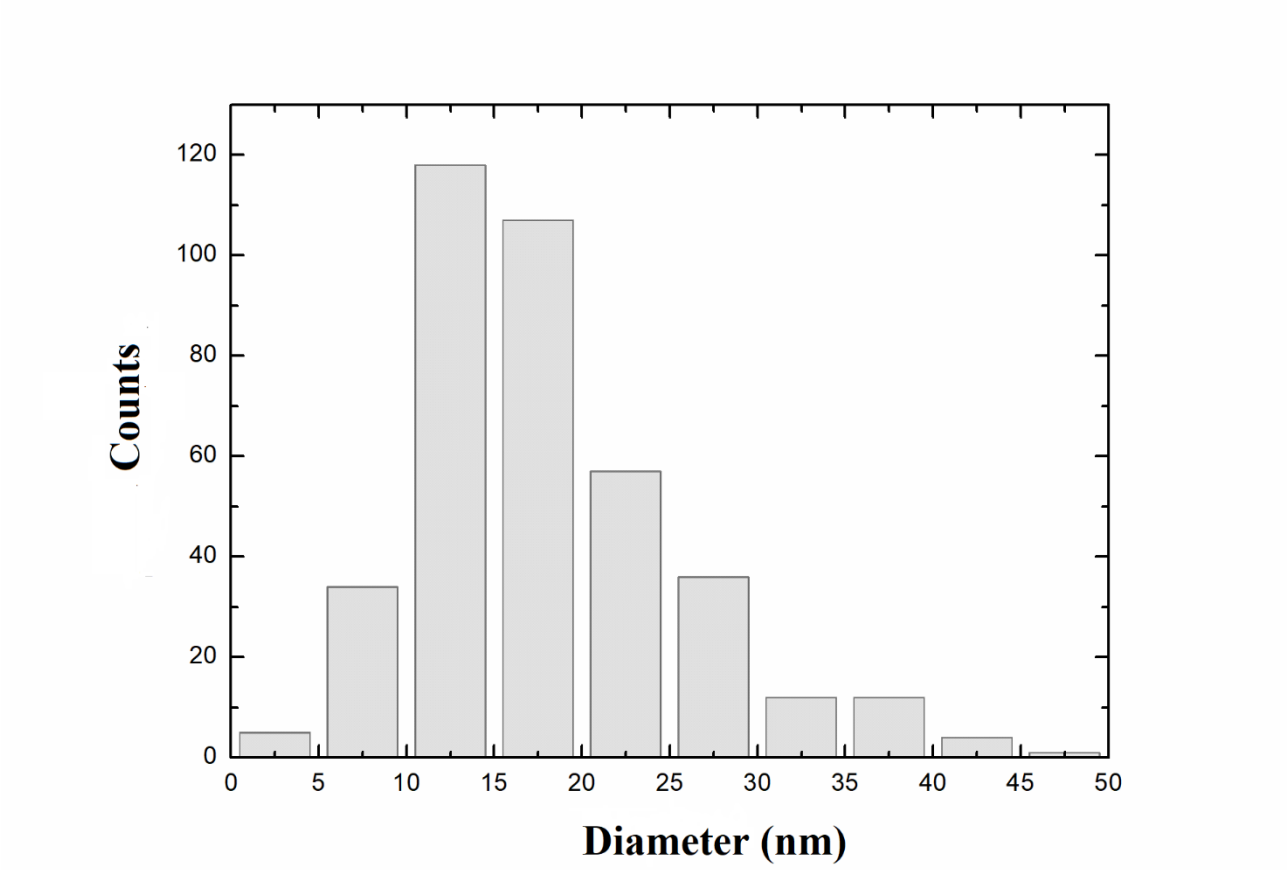

Fig. S5 Size distribution of the globular structures imaged by AFM upon deposition on mica of a freshly-prepared 30 μM SMG aqueous solution (phosphate buffer, pH 8, T=25°C).

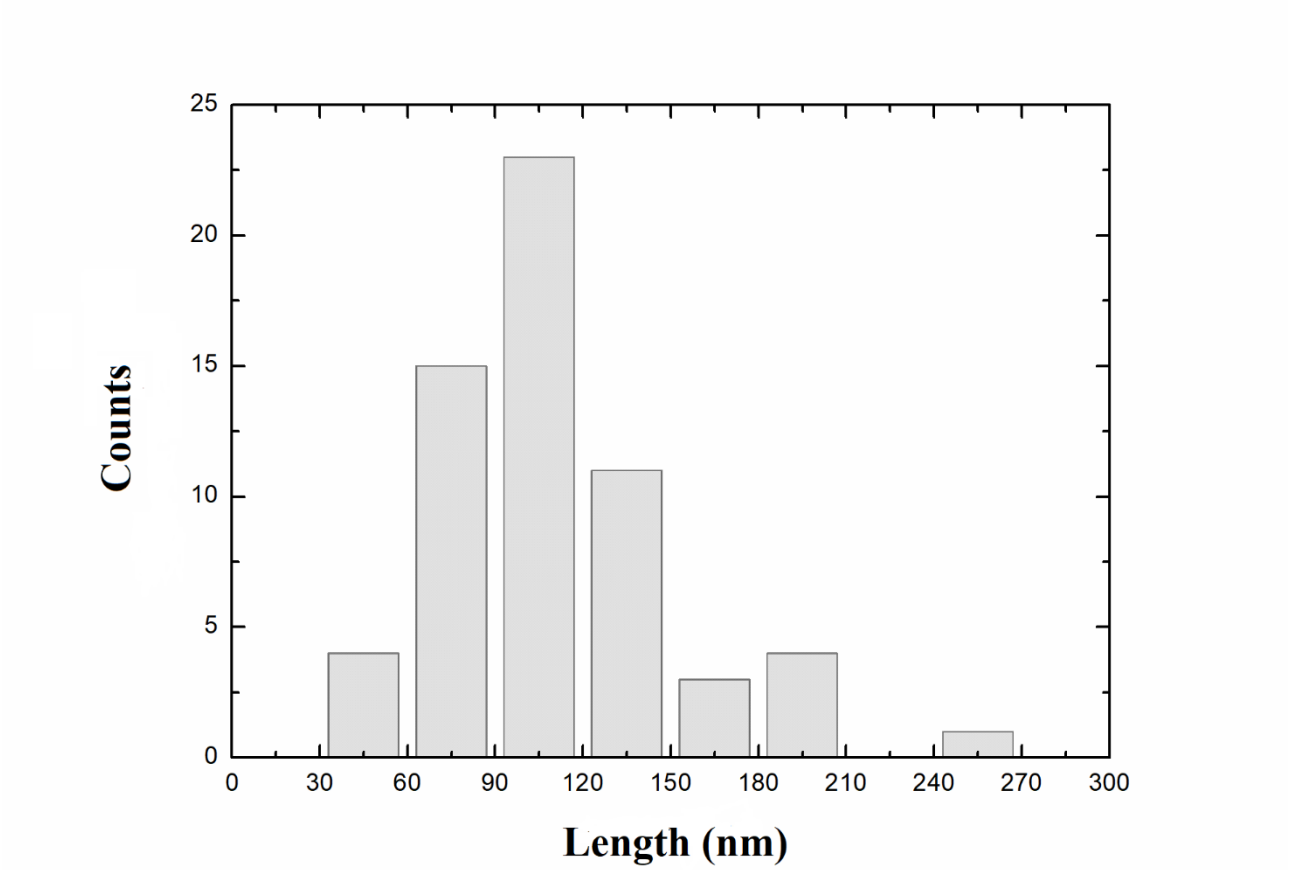

Fig. S6 Size distribution (length) of the rod structures imaged by AFM upon deposition on mica of an aged 30 μM SMG aqueous solution (phosphate buffer, pH 8, T=25°C).

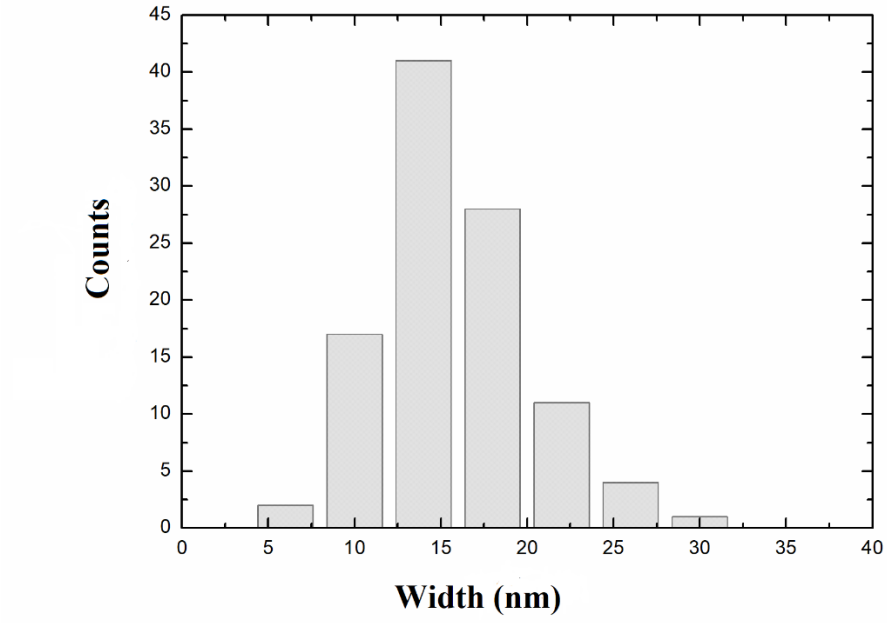

Fig. S7 Size distribution (width) of the rod structures imaged by AFM upon deposition on mica of an aged 30 μM SMG aqueous solution (phosphate buffer, pH 8, T=25°C).

Table T1 Time decay parameters of SMG in water/glycerol 1:2 (v/v) solutions for different temperatures.

T(°C)	**τ_1 (ns)**	**α_1**	**τ_2 (ns)**	**α_2**	**τ_3 (ns)**	**α_3**	**$\langle\tau\rangle$ (ns)**
3.1	0.88	0.23	4.38	0.43	7.59	0.34	4.7
5.8	0.82	0.23	4.62	0.52	7.88	0.25	4.6
10.0	0.91	0.22	4.54	0.54	7.74	0.24	4.5
14.8	0.74	0.20	4.24	0.54	7.59	0.26	4.4
20.7	0.83	0.20	4.15	0.58	7.51	0.22	4.3
25.2	0.97	0.18	4.17	0.62	7.62	0.20	4.3
29.8	0.99	0.20	4.17	0.64	7.73	0.16	4.1
34.4	1.11	0.20	4.04	0.63	7.54	0.17	4.1

Table T2. Fluorescence time decays of SMG aged solutions (phosphate buffer, pH 8, T=25°C

λ_{ex}=298 nm; λ_{em} = 350 nm

Concentration (μM)	α_1	τ_1 (ns)	α_2	τ_2 (ns)	α_3	τ_3 (ns)	$\langle\tau\rangle$ (ns)	χ^2
4	0.89	1.2	0.05	3.7	0.06	9.9	1.9	1.04
20	0.74	0.7	0.24	3.3	0.02	13.6	1.7	1.09
30	0.80	1.4	0.14	5.6	0.06	13.8	2.7	1.12

λ_{ex}=298 nm; λ_{em} = 420 nm

Concentration (μM)	α_1	τ_1 (ns)	α_2	τ_2 (ns)	$\langle\tau\rangle$ (ns)	χ^2
4	0.25	0.94	0.75	3.72	3.02	2.71
20	0.35	0.89	0.65	3.85	2.82	2.77
30	0.18	0.34	0.82	3.33	2.80	2.59

λ_{ex}=344 nm; λ_{em} = 420 nm

Concentration (μM)	α_1	τ_1 (ns)	α_2	τ_2 (ns)	α_3	τ_3 (ns)	$\langle\tau\rangle$ (ns)	χ^2
4	0.35	1	0.2	3.1	0.45	6.2	3.8	1.06
20	0.54	0.2	0.17	1.7	0.29	5.5	2.0	1.12
30	0.44	1.2	0.47	4.7	0.09	10.5	3.8	1.12

Fractal autocatalytic aggregation model (Pasternack *et al.* 1998):

$$\lambda(t) = \lambda_0 + \frac{(\lambda_0 - \lambda_i)}{\left\{1 + (m-1)\left[k_0 t + \frac{(k_c t)^{n+1}}{n+1}\right]\right\}^{\frac{1}{m-1}}}$$

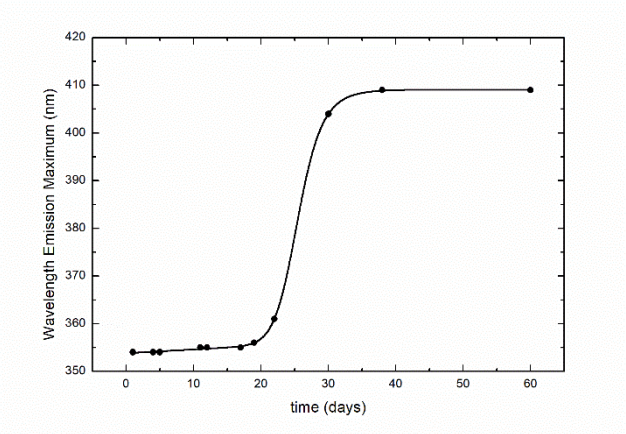

Parameter	Value	Standard Error
λ_i (nm)	409.1	0.2
λ_0 (nm)	353.8	0.2
m	2.1	0.6
n	14	3
k_0 (d^{-1})	1.5×10^{-3}	4×10^{-4}
k_c (d^{-1})	4.72×10^{-2}	4×10^{-4}
$\chi^2 = 0.0673$		$R^2 = 0.9999$

TOR VERGATA
UNIVERSITÀ DEGLI STUDI DI ROMA

Dipartimento di Scienze e Tecnologie Chimiche

Rome, May 30th 2020

Dear Prof. Banerjee, Dear Referee,

here attached you can find a research article paper that I would like to submit for the Special Issue 'Peptide Soft Materials' to be published on Soft Matter.

Title of the submitted contribution is: 'A spectroscopic and molecular dynamics study on the aggregation process of a long-acting lipidated therapeutic peptide: the case of Semaglutide',

authored by: M. Savioli, R. Cimino, E. Gatto, A. Palleschi, G. Ripani, D. Cicero (University of Rome Tor Vergata, Italy); E. Placidi (University of Rome 'La Sapienza', Italy); F. Orvieto, E. Bianchi (IRBM, Pomezia, Italy).

In the paper we describe the aggregation properties of Semaglutide, a peptide drug recently approved for therapeutic treatment of diabete type 2, and commercialized by Novo Nordisk (Ozempic).

We applied optical spectroscopy (Circular dichroism, steady-state and time-resolved fluorescence), Molecular Dynamics simulations and Atomic Force Microscopy imaging to study the aggregation properties of Semaglutide from the very early steps to the formation, at very long times, of mesoscopic structures.

We found that Semaglutide remains for a very long time (days) in an oligomeric state, forming predominantly monomers, less frequently dimers, and only sporadically trimers. Most likely this behaviour is the basis for the prolonged hemi-life of Semaglutide in the blood, as the monomeric state promotes the binding to human serum albumin. We show by MD simulations that the two PEG units and C18 fatty acid chain are also important to stabilize the globular structure of Semaglutide monomers and dimers.

We also show that, at very long times (weeks), these oligomeric clusters nucleate the growth of nanostructured aggregates, characterized by blue luminescence, β-sheet organization of the peptide chains, and rod-shaped building blocks and gorgonian-like morphology.

In the paper, we show that the dendrimeric morphology of these aggregates results from a hierarchical self-assembly process, that starts from the Semaglutide oligomers and evolve, cooperatively, to the final micrometric structure.

I hope that you can find this contribution appropriate for the 'Peptide Soft Materials' Special Issue and of interest for the readership of Soft Matter.

I would like to thank you for kind attention.

Via della Ricerca Scientifica, 1
www.stc.uniroma2.it

Tel. 06 72594337
Email: chimica@uniroma2.it

TOR VERGATA
UNIVERSITÀ DEGLI STUDI DI ROMA

Dipartimento di Scienze e Tecnologie Chimiche

Best regards

Prof. Mariano Venanzi
Chair of Physical Chemistry
Dept. of Chemical Science and Technologies
University of Rome Tor Vergata
Rome, Italy.
e-mail: venanzi@uniroma2.it
mobile: (+39) 3331594471

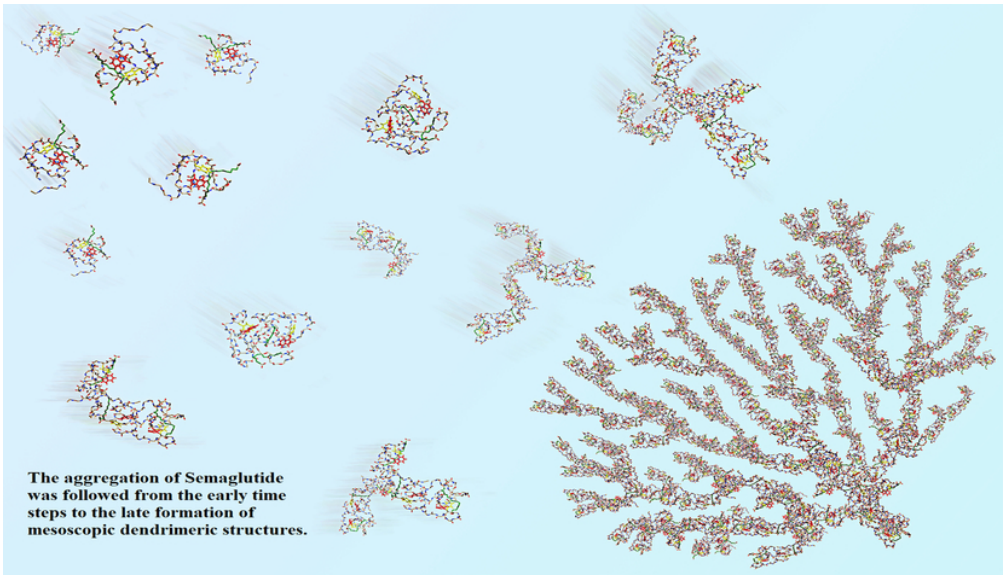

70x40mm (300 x 300 DPI)